

DRINet++: Efficient Voxel-as-point Point Cloud Segmentation

Maosheng Ye^{1‡*} Rui Wan^{2*} Shuangjie Xu^{1‡} Tongyi Cao² Qifeng Chen¹
¹Hong Kong University of Science and Technology ²DEEPROUTE.AI
myeag, ssubj@connect.ust.hk {ruiwan, tongyicao}@deeproute.ai cqf@ust.hk

Abstract

Recently, many approaches have been proposed through single or multiple representations to improve the performance of point cloud semantic segmentation. However, these works do not maintain a good balance among performance, efficiency, and memory consumption. To address these issues, we propose DRINet++ that extends DRINet by enhancing the sparsity and geometric properties of a point cloud with a voxel-as-point principle. To improve efficiency and performance, DRINet++ mainly consists of two modules: Sparse Feature Encoder and Sparse Geometry Feature Enhancement. The Sparse Feature Encoder extracts the local context information for each point, and the Sparse Geometry Feature Enhancement enhances the geometric properties of a sparse point cloud via multi-scale sparse projection and attentive multi-scale fusion. In addition, we propose deep sparse supervision in the training phase to help convergence and alleviate the memory consumption problem. Our DRINet++ achieves state-of-the-art outdoor point cloud segmentation on both SemanticKITTI and Nuscenec datasets while running significantly faster and consuming less memory.

1. Introduction

Large-scale outdoor point cloud segmentation has been a crucial task for autonomous driving systems and has demanding requirements for efficiency, performance, and memory consumption. For point cloud segmentation, PointNet [31] and PointNet++ [32] are the pioneering works that directly operate on a point cloud to learn pointwise features by utilizing the key geometric properties (e.g., permutation invariant, Euclidean distances) of a point cloud. However, it is hard to apply these approaches in outdoor scenarios due to high memory consumption and low runtime efficiency. RandLA [15] applies a random sampling strategy to reduce the number of points to improve efficiency, which leads to some information loss. With the pop-

[‡]Part of the work was done during an internship at DEEPROUTE.AI.

*Equal contributions.

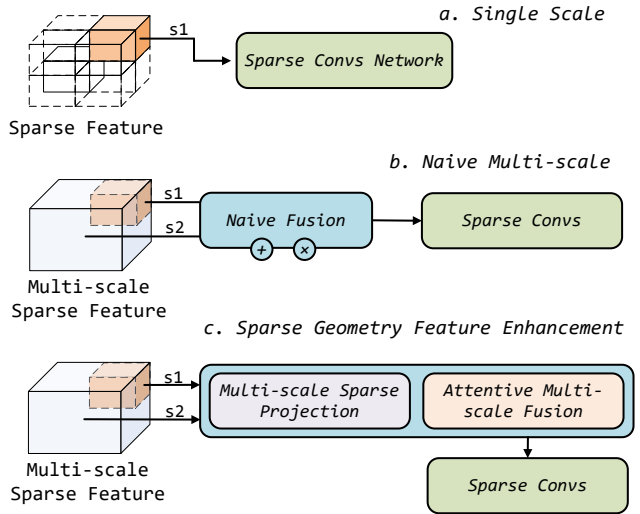


Figure 1. Comparison between two common ways to deal with sparse features and our proposed method.

ularity of sparse convolutions [11, 52], there has been some progress in utilizing the sparse voxel-based representation (e.g., AF2S3Net [6] and Cylinder3D [62]), which is a representation that preserves the 3D Euclidean space. Compared with point-based representations, the merits of the sparse voxel-based representation lie in the effectiveness and efficiency in quickly expanding the receptive fields based on the sparsity of a point cloud (another key property). Furthermore, the sparse voxel-based representation, which aggregates point features within the local neighborhood, can significantly reduce memory usage. Also, traditional or current popular convolutional neural networks (CNNs) can be directly applied to extract better context information.

Recently, several works recognize the limitation of a single representation and explore richer information by synergizing multiple representations. PVCNN [23] fuses point-based and voxel-based representations with MLP layers and dense 3D convolution layers but does not take point cloud sparsity into consideration. SPVCNN [38], TPCN [54] and DRINet [56] design the sparse convolution layers and pointwise operational layers to fuse features considering sparsity and geometry. Furthermore, RPNNet [49] combines the

range-view, point, and voxel representations for point cloud segmentation. The general framework of current multi-representation learning is to utilize sparse convolutions for locality and sparsity, and pointwise operations for geometry learning, aiming to combine sparsity and geometry for a better balance between performance and efficiency. While these approaches lead to some performance improvements, the extra computation cost and memory usage brought by the additional point representation cannot be ignored considering 100K points. Meanwhile, according to the experimental results by these approaches [38,56], the voxel-based representation is still the dominant one, with which these methods do achieve decent performance. Note that a voxel can be a “**super point**” as the abstraction of a set of points within a cube, and the number of voxels can be much less than the number of points as shown in Fig. 3. Therefore, we are raising a question: Is it enough to only keep voxel-based representation and treat the voxels as points for efficiency, and apply these pointwise operations to the “**super points**” for better performance? Inspired by these observations, we propose DRINet++ to explore extra geometric properties based on a single sparse voxel-based representation. We extend the architecture from DRINet [56] for its merits in iterative learning, and redesign the pointwise operations based on the principle of “**voxels as points**”. Compared with these multi-representation methods, our DRINet++ incorporates sparsity and geometric properties of a point cloud in a unified representation without introducing extra computation cost from multi-representation fusion.

Our DRINet++ extends the design of DRINet [56] and mainly contains two modules to iteratively enhance feature learning: Sparse Feature Encoder (SFE) and Sparse Geometric Feature Enhancement (SGFE). Each module takes the output of the other module as input to fully explore the sparsity and geometric properties of a point cloud at a low computation cost and memory usage. In SGFE (shown in Fig. 1), we propose a novel multi-scale sparse projection layer for hierarchical geometry learning and attentive multi-scale fusion for multi-scale feature selection. Apart from that, we apply deep sparse supervision compared with the most common dense manner to alleviate the pressure of memory consumption. Compared with DRINet [56], our DRINet++ treats the voxels as points to alleviate the memory and efficiency problem.

Our contributions are summarized as follows:

- We propose a new lightweight network architecture called DRINet++ based on the voxel-as-point principle to fully exploit the sparsity and geometry properties of a point cloud. The Multi-scale Sparse Projection and the Attentive Multi-scale Fusion in the Sparse Geometric Feature Enhancement are proposed to enhance geometric feature learning.

- Deep Sparse Supervision is proposed as a training strategy in a deep and sparse fashion to reduce the memory cost and improve the performance.
- We evaluate our proposed approach on large-scale outdoor scenario datasets including SemanticKITTI [1] and nuScenes-lidarseg [3] to demonstrate the effectiveness of our method. We achieve state-of-the-art performance on both datasets with an average running time of 59ms per frame with an Nvidia RTX 2080Ti GPU.

2. Related Work

Indoor Point Cloud Segmentation. The point cloud from an indoor scene often has closely positioned points with a small range. The existing indoor point cloud segmentation approaches can be classified according to their model representations. For point-based approaches, PointNet [31], PointNet++ [31], and their related works [21, 22, 30, 33, 47, 57] based on a similar architecture are popular models in this task. Most of these works explore the local neighborhood context while preserving the inherent geometry of a point cloud. They use different grouping and permutation invariant operations to promote performance. The other mainstream methods [17, 18, 23, 27, 36] follow the volumetric representation by partitioning the space as discrete pixels/voxels and then apply 2D/3D CNN architecture to the regular representation. Graph-based approaches for point cloud learning [40, 43–45, 50, 58] are also popular due to the nature of graph to deal with unorderedness and the capability to model the relationship among points. Currently, with the popularity of transformers, some works [12, 60] achieve state-of-the-art performance in indoor point cloud learning by introducing transformer-based architectures. Although a number of novel architectures have been proposed to improve point cloud learning, some of them fail to generalize to outdoor scenarios with thousands of hundreds of points.

Outdoor Point Cloud Segmentation. Compared with indoor point cloud segmentation, the sparsity and larger number of points pose great challenges for existing approaches. Point-based methods such as KPConv [41] and RandLA [15] extend the architecture of PointNet [31] or PointNet++ [32] and adopt sampling strategies to alleviate these problems but lead to extra information loss. KPConv [41] introduces the kernel point selection process to generate high-quality sampling points. Range-view-based approaches [8, 46, 48] project the point cloud into range views or spherical representations and apply efficient CNN architectures. However, the range view cannot maintain the metric space and introduces distortions, which potentially leads to performance degradation. Some other approaches [6, 7, 51, 59, 62] quantize a point cloud into some pre-defined space or representations (e.g., polar grids, 2D grids, and sparse 3D grids) and then apply regular convo-

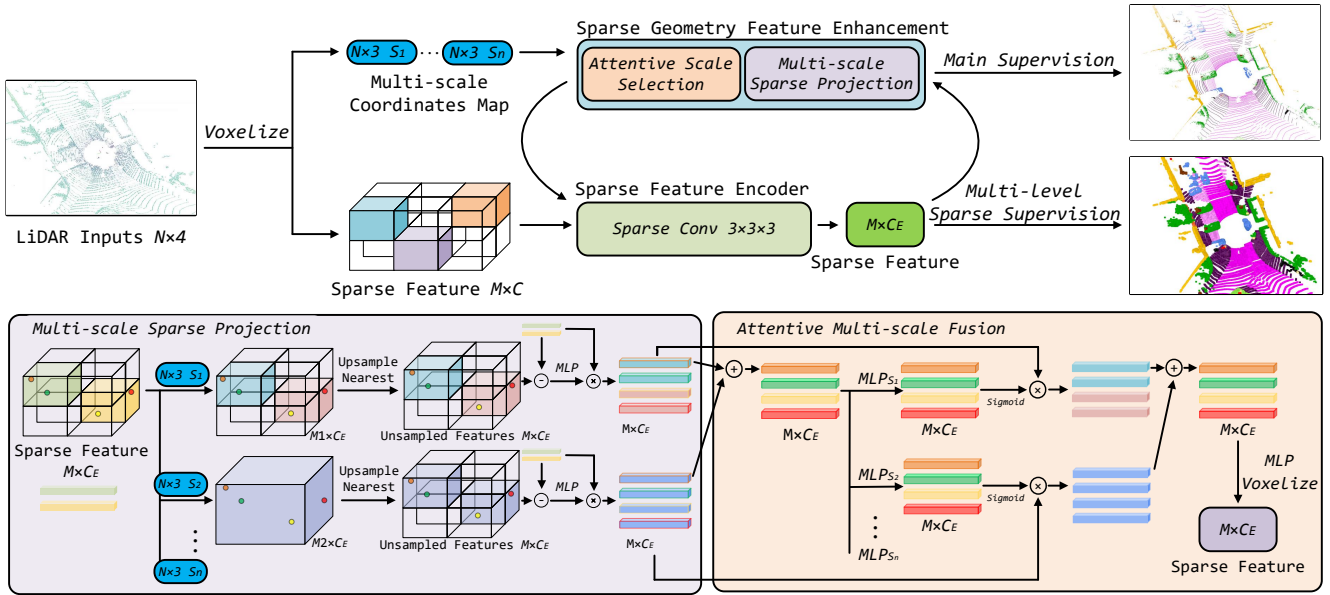


Figure 2. The overall structure of our DRINet++. In the top half of the figure, LiDAR input is firstly voxelized as sparse features. Then the Sparse Feature Encoder utilizes sparse convolutions to process the sparse features. Furthermore, Sparse Geometry Feature Enhancement will enhance the features by Multi-scale Sparse Projection and Attentive Multi-scale Fusion layer to generate the input of Sparse Feature Encoder at the next stage. Sparse supervision will be attached to the output of the sparse feature encoder as an auxiliary loss. The bottom line describes the details about Multi-scale Sparse Projection and Attentive Multi-scale Fusion. N is the number of points, M_i is the number of voxels for i -th scale, C_E is the channel dimension.

lution neural networks or sparse convolutions [11, 52] to achieve the balance between efficiency and performance. A line of works integrates the multiple representations, including range views, voxel representations, and point representation, to exploit the potential of different representations deeply [23, 38, 49, 56]. These works utilize different architectures for different representations and propose various fusion strategies and show strong performance gain compared to single-representation-based methods, at the cost of extra running time.

Image Segmentation to Point Cloud Segmentation. The fully convolutional network (FCN) [24] is one of the pioneering works for image segmentation with deep learning. Based on FCN and existing prevalent CNN architecture, DeepLab [4], PSPNet [61] and their following works [5, 53] are proposed with multi-scale or multiple dilation rate strategies to explore more hierarchical local context information. Furtherly, HRNet [37] fuses different resolution heatmap in a single framework and keeps the high resolution to improve the performance. Considering the great process achieved in image segmentation, lots of works [28, 42, 56, 59, 62] have applied these tricks including hierarchy learning, attention mechanism, or backbones into point cloud segmentation. Some works [7, 62] are built on U-net [34] with sparse convolution acceleration.

3. Approach

The overall network architecture of our DRINet++ is based on DRINet [55] that propagates features in an iter-

ative manner, but only consists of two different modules: 1) Sparse Feature Encoder 2) Sparse Geometry Feature Enhancement. Sparse Feature Encoder serves as a basic block for fast local context aggregation. Sparse Geometry Feature Enhancement, which takes the output of Sparse Feature Encoder as input, enhances the geometric information by multi-scale sparse projection and attentive multi-scale fusion layer. Both modules interact a proposed voxel-as-point fashion to reduce computation cost and improve runtime efficiency. Compared with previous multi-representation methods [23, 38, 56], we treat the voxels as points and apply geometric operations to mimic the previous pointwise feature learning. Moreover, we propose to apply Deep Sparse Supervision at the voxel level to alleviate the memory issues resulted from dense supervision in sec. 3.4. Fig. 2 demonstrates the overall framework of our proposed approach. Limitations are discussed in the supplementary materials.

3.1. Voxels As Points

The dual representation learning in DRINet [56] and SPVCNN [38] includes both pointwise features and voxelwise features. However, the memory consumption increases significantly with more pointwise operations. One key observation is that larger-size voxels contain more points, as shown in Fig. 3, meaning that the number of voxels will greatly decrease with coarser voxels while the number of the points number keeps the same. Another intuition is that voxelwise features are aggregated features within a local neighborhood, which implicitly implies pointwise ge-

ometry. Based on these two observations, we can treat each voxel as a special type of “**super point**” and apply pointwise operations on voxels namely “**voxels as points**”, which can reduce memory cost and improve performance with the pointwise operations. By treating voxels as points, we integrate sparsity and geometry in a novel and efficient way, which is applicable in any multi-representation learning framework. We conduct experiments in sec.4.4 in several multi-representation approaches to verify this principle.

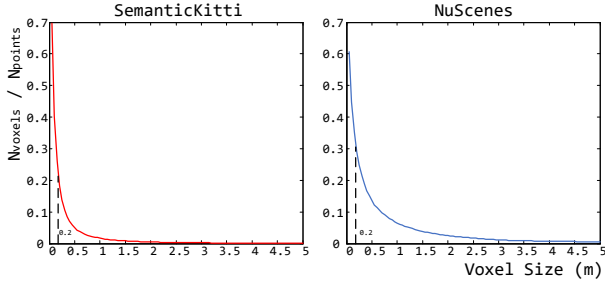


Figure 3. The variation curve of the ratio of voxel number (N_{voxels}) to point number (N_{points}) against voxel size.

3.2. Sparse Feature Encoder

The sparse voxel representation makes it easy to apply standard convolution operations to extract local context information. Thus, we utilize sparse convolution layers [11, 52] instead of dense convolution [23]. One merit of sparse convolution lies in the sparsity, with which the convolution operation only considers the non-empty voxels. Based on this, we build our sparse feature encoder (SFE) with sparse convolutions to quickly expand the receptive field with less computation cost. We adopt the ResNet BottleNeck [13] while replacing the ReLU activation with Leaky ReLU activation [26] compared with DRINet [56] and SPVCNN [38]. In order to keep a high efficiency, all the channel number for sparse convolution is set to 64.

3.3. Sparse Geometry Feature Enhancement

After obtaining the sparse voxelwise features from the sparse feature encoder, we aim to enhance the voxelwise features with more geometric guidance by our Sparse Geometry Feature Enhancement (SGFE).

Multi-scale Sparse Projection (MSP). Inspired by previous works [32, 56, 61] that focus on multi-scale features aggregation, we notice that hierarchical context information helps enhance the capability of feature extraction, especially for point clouds. Multi-scale features bring point cloud learning more geometric enhancement since each voxel scale reflects one specific physical dimension property. However, it is not applicable to directly apply Pyramid Pooling Module from PSPNet [61] due to the sparsity of point cloud. DRINet [56] proposes points max pooling at point level by scattering operation while introducing extra

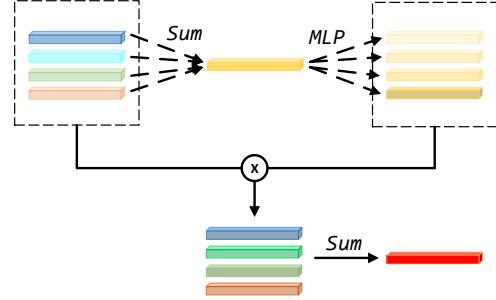


Figure 4. An example demonstrates the Attentive Multi-scale Fusion. \otimes means tensor elementwise multiplication.

Algorithm 1 Multi-scale Sparse Projection

Input: Input sparse voxel features F and pre-defined scale set S

Output: Multi-scale features O

- 1: $L = []$
 - 2: **for each** $s \in S$ **do**
 - 3: $V^s = \text{AvgPooling}(F, s)$
 - 4: $O^s = F - \text{UpsampleNearest}(V^s)$
 - 5: $O^s = \text{MLP}(O^s) * F$
 - 6: $L.append(\text{MLP}(O^s))$
 - 7: **end for**
 - 8: $O \leftarrow \text{Stack}(L)$
 - 9: **return** O
-

huge memory cost and resulting in information loss. As a result, we propose **Multi-scale Sparse Projection** layer to exploit the multi-scale features at a sparse voxel level through voxels as points, with a lower memory cost.

Given the input voxelwise features F and pre-defined scale set S , Multi-scale Sparse Projection is described in Algo. 1. For each scale, we project the features into local regions to get projection mean embedding with different local geometric priors. Then features shift that is calculated based on the projection embedding will be treated as the kernel weighted function like KPConv [41] to strengthen input features. This enforces similar features share similar weights for more consistent local geometry. Finally, features at different scales are stacked together.

Attentive Multi-scale Fusion (AMF). After obtaining the multi-scale features from the multi-scale sparse projection layer, a naive way of multi-scale features fusion is to apply tensor concatenation or summation. As such, all the features from different scales share the same weights and are treated equally. We believe that the features from different scales contain different geometric priors and represent a scene hierarchically. From this point of view and motivated by the SENet [14] and SKNet [20], a better approach to fusing multi-scale features is to apply re-weighting strategy along scale dimension for each feature channel to re-

Algorithm 2 DRINet++

Input: Input sparse voxel features F , the number of blocks B , and the target scale s

Output: Semantic prediction P

```
1:  $L = []$ 
2:  $Loss = 0$ 
3: for  $i = 1$  to  $B$  do
4:    $V \leftarrow \text{SFE}(F)$ 
5:    $F \leftarrow \text{SGFE}(V)$ 
6:    $O^s \leftarrow \text{UpsampleNearest}(F, s)$ 
7:    $Loss += \text{LossFunc}(V)$ 
8:    $L.append(O^s)$ 
9: end for
10:  $L \leftarrow \text{Stack}(L)$ 
11:  $P = \text{Softmax}(\text{MLP}(L))$ 
12: return  $P$ 
```

distribute the importance of each scale.

As shown in Fig. 4, we first sum over all the input tensors in the first-stage fusion to collect all the information from different scales. Inspired from current popular attention works [20], we apply a multi-scale MLP layer with sigmoid activation for the results to get the attentive embedding for each scale. Finally, tensor multiplication between attention weight tensor and multi-scale features is applied, followed by the tensor summation among multi-scale features. Compared with AF2S3Net [6], our Attentive Multi-scale Fusion is more lightweight without introducing extra convolution layers and is only operated at the voxel with the voxel-as-point principle for better efficiency.

3.4. Deep Sparse Supervision

Dense supervision on each pixel/voxel is a popular way in both 2D and 3D semantic segmentation tasks. Previous methods [59, 62] generate dense feature maps with dense supervision. Although these works have considered the sparsity with their network architectures, they ignore this property when designing the loss, one of the key differences between 2D and 3D data. In fact, dense supervision with fine-grained feature maps brings a significant overload on memory usage. For example, when using a grid size of $0.2m$, the memory consumption (about 500 Mb) for a single dense feature map with 20 classes could be problematic. Based on these observations and inspired by [25], we propose a novel **Deep Sparse Supervision (DSS)** to deal with supervision in a deep sparse style.

Since we stack multiple blocks of SFE to generate sparse voxelwise features at different scales, we apply sparse supervision to the output voxelwise features stage by stage as a deep auxiliary loss. We also apply sparse supervision for the main final prediction branch. The auxiliary loss helps optimize the training, while the main branch loss accounts

for the most gradients.

In the testing stage, all the auxiliary branches are disabled to keep the runtime efficiency. This training strategy has been proven its effectiveness in image-based segmentation [24]. We consider the sparsity of point cloud and apply it in a sparse manner to save memory consumption.

3.5. Final Prediction

For the final semantic prediction, we fuse the multi-stage features from the output of each Sparse Geometry Feature Enhancement Layer by nearest upsampling to the most fine-grained scale of the voxel. To obtain pointwise results, we also apply the nearest interpolation strategy, with which each point is attached with the semantic features from the voxel that it lies in. The whole algorithm for our framework is illustrated in Algo. 2.

4. Experiments

4.1. Experimental Setup

We conduct experiments on two large-scale outdoor datasets, SemanticKITTI [1] and Nuscenet [3], to evaluate our proposed approach.

SemanticKITTI [1]. The SemanticKITTI dataset is generated from the KITTI dataset [10] and contains 22 sequences that involve common scenes for autonomous driving. Each scan in the dataset has more than 100K points on average with pointwise annotation labels for 20 classes. According to the official settings, sequences from 00 to 10 except 08 are the training split, sequence 08 is the validation split, and the rest sequences from 11 to 21 are the test split.

Nuscenet [3]. The Nuscenet dataset has a total of 40,000 scans collected by a 32-beam LiDAR. Compared with SemanticKITTI [1], it contains fewer points and annotations classes (16 classes).

Both datasets use **mIoU** as one evaluation metric, which is popular in point cloud semantic segmentation. In addition, SemanticKITTI provides the average accuracy metric **Acc**, and Nuscenet uses **fwIoU** as additional criteria, which is the weighted sum of IoU for each class based on point-level frequencies.

Network Details. We use the same setting for both datasets. We discretize a point cloud with a voxel scale of $0.2m$ along xyz dimensions to generate the initial sparse voxel features. Our DRINet++ has four blocks of Sparse Feature Encoder and Sparse Geometry Feature Enhancement. In the ablation study, we also evaluate the effect of block number choice between performance and efficiency. As for the multi-scale sparse projection layer, we adopt kernel sizes and strides both with [2, 4, 8, 16], which could cover the coarse and the fine pooling regions. Similar to previous works, we apply random flipping, random point dropout, random scale, and global rotation in the training

Methods	road	sidewalk	parking	other ground	building	car	truck	bicycle	motorcycle	other vehicle	vegetation	trunk	terrain	person	bicyclist	motorcyclist	fence	pole	traffic sign	mIoU	speed (ms)
PointNet [31]	61.6	35.7	15.8	1.4	41.4	46.3	0.1	1.3	0.3	0.8	31.0	4.6	17.6	0.2	0.2	0.0	12.9	2.4	3.7	14.6	500
PointNet++ [32]	72.0	41.8	18.7	5.6	62.3	53.7	0.9	1.9	0.2	0.2	46.5	13.8	30.0	0.9	1.0	0.0	16.9	6.0	8.9	20.1	5900
KPConv [41]	88.8	72.7	61.3	31.6	90.5	96.0	33.4	30.2	42.5	44.3	84.8	69.2	69.1	61.5	61.6	11.8	64.2	56.4	47.4	58.8	-
RandLA [15]	90.7	73.7	60.2	20.4	86.9	94.2	40.1	26.0	25.8	38.9	81.4	66.8	49.2	49.2	48.2	7.2	56.3	47.7	38.1	53.9	880
SqueezeSegV3 [48]	91.7	74.8	63.4	26.4	89.0	92.5	29.6	38.7	36.5	33.0	82.0	58.7	65.4	45.6	46.2	20.1	59.4	49.6	58.9	55.9	238
RangeNet++ [29]	91.8	75.2	65.0	27.8	87.4	91.4	25.7	25.7	34.4	23.0	80.5	55.1	64.6	38.3	38.8	4.8	58.6	47.9	55.9	52.2	83.3
TangentConv [39]	83.9	63.9	33.4	15.4	83.4	90.8	15.2	2.7	16.5	12.1	79.5	49.3	58.1	23.0	28.4	8.1	49.0	35.8	28.5	35.9	3000
SPVCNN [38]	90.2	75.4	67.6	21.8	91.6	97.2	56.6	50.6	50.4	58.0	86.1	73.4	71.0	67.4	67.1	50.3	66.9	64.3	67.3	67.0	259
PolarNet [59]	90.8	74.4	61.7	21.7	90.0	93.8	22.9	40.3	30.1	28.5	84.0	65.5	67.8	43.2	40.2	5.6	61.3	51.8	57.5	54.3	62
DASS [42]	92.8	71.0	31.7	0.0	82.1	91.4	66.7	25.8	31.0	43.8	83.5	56.6	69.6	47.7	70.8	0.0	39.1	45.5	35.1	51.8	90
JS3C-Net [51]	88.9	72.1	61.9	31.9	92.5	95.8	54.3	59.3	52.9	46.0	84.5	69.8	67.9	69.5	65.4	39.9	70.8	60.7	68.7	66.0	-
DRINet [56]	90.7	75.2	65.0	26.2	91.5	96.9	43.3	57.0	56.0	54.5	85.2	72.6	68.8	69.4	75.1	58.9	67.3	63.5	66.0	67.5	62
Cylinder3D [62]	92.0	70.0	65.0	32.3	90.7	97.1	50.8	67.6	63.8	58.5	85.6	72.5	69.8	73.7	69.2	48.0	66.5	62.4	66.2	68.9	131
AF2S3Net [6]	92.0	76.2	66.8	45.8	92.5	94.3	40.2	63.0	81.4	40.0	78.6	68.0	63.1	76.4	81.7	77.7	69.6	64.0	73.3	70.8	-
RPVNet [49]	93.4	80.7	70.3	33.3	93.5	97.6	44.2	68.4	68.7	61.1	86.5	75.1	71.7	75.9	74.4	43.4	72.1	64.8	61.4	70.3	168
Ours	89.8	74.6	66.2	30.1	92.3	96.9	59.3	65.8	58.0	61.0	87.3	73.0	72.5	80.4	82.7	46.3	69.6	66.1	71.6	70.7‡	59

Table 1. The per-class mIoU results on the SemanticKITTI test set. ‡ donates the second best results. All results are obtained from the literature or leaderboard, including standard Test-Time Augmentation.

Method	mIoU	Acc
Cylinder3D [62]	52.5	91.0
TemporalLidarSeg [9]	47.0	-
KPConv [41]	51.2	89.3
LatticeNet [35]	45.2	89.3
AF2S3Net [6]	56.9	88.1
Ours	61.3	92.4

Table 2. Comparison to the state-of-the-art methods on the test set of SemanticKITTI multiple scans challenge.

stage. Besides that, motivated by the improvement achieved by Pseudo Label [19] in semi-supervised learning, we apply this technique for our data augmentation. First, we train our model on the training set, and then we predict the pointwise label for the validation set as the Pseudo label. After merging the training set and validation set with pseudo labels, we train our model with this mixture dataset to improve the performance. For the loss design, we follow Cylinder3D [62] to combine the Lovasz loss [2] and cross-entropy loss as supervision. Adam optimizer [16] is employed with an initial learning rate of $2e^{-3}$ at batch size 4 for 50 epochs. Learning rate decays in a ratio of 0.1 for every 15 epochs.

4.2. Results on SemanticKITTI

We provide the detailed per-class quantitative results of our DRINet++ as well as other state-of-the-art methods in Tab. 1. Compared with previous methods, DRINet++ achieves state-of-the-art performance while maintaining real-time inference efficiency. Although DRINet++ fails to

Method	Param (M)	Macs (G)	Speed	Memory	mIoU
SPVCNN	12.5	73.8	120 ms	2.4 Gb	67.0
DRINet	3.5	14.58	62* ms	2.1* Gb	67.5
Cylind3D	53.3	64.3	131 ms	3.0 Gb	68.9
RPVNet	24.8	119.5	168* ms	2.7* Gb	70.3
Ours	2.2	12.1	59 ms	1.4 Gb	70.7

Table 3. Quantitative results of model complexity with the performance from the leaderboard of SemanticKITTI on the test set. Statistics of the number of parameters and Macs are from the corresponding papers. The speed of each method is evaluated on a single Nvidia RTX 2080Ti GPU. * donates the statistics are from our reproduction.

achieve the best result for every class, it achieves balanced results among all the classes. Even compared to multiple representation fusion approaches [38, 49, 56], our method still surpasses by a considerable margin.

Furthermore, we also provide quantitative analysis for the model complexity and latency for some state-of-the-art methods and our DRINet++ in Tab. 3 to illustrate the high performance-time ratio of our approach. Compared with previous methods, we achieve the best mIoU result with the least computation cost, demonstrating the efficiency and effectiveness of our approach. Some qualitative results on the SemanticKITTI validation set are shown in Fig. 5.

Multiple Scans. Meanwhile, we also conduct experiments on SemanticKITTI multiple scans challenge to verify the effectiveness of our DRINet++. In this task, we directly stack multiple aligned scans as input without any

Method	barrier	bicycle	bus	car	construction	motorcycle	pedestrian	traffic cone	trailer	truck	driveable	other_flat	sidewalk	terrain	manmade	vegetation	FW mIoU	mIoU
AF2S3Net [6]	78.9	52.2	89.9	84.2	77.4	74.3	77.3	72.0	83.9	73.8	97.1	66.5	77.5	74.0	87.7	86.8	88.5	78.3
Cylinder3D [62]	82.8	29.8	84.3	89.4	63.0	79.3	77.2	73.4	84.6	69.1	97.7	70.2	80.3	75.5	90.4	87.6	89.9	77.2
SPVCNN [38]	80.0	30.0	91.9	90.8	64.7	79.0	75.6	70.9	81.0	74.6	97.4	69.2	80.0	76.1	89.3	87.1	89.7	77.4
PolarNet [59]	72.2	16.8	77.0	86.5	51.1	69.7	64.8	54.1	69.7	63.5	96.6	67.1	77.7	72.1	87.1	84.5	87.4	69.4
Ours	85.5	43.2	90.5	92.1	64.7	86.0	83.0	73.3	83.9	75.8	97.0	71.0	81.0	77.7	91.6	90.2	91.0	80.4

Table 4. The per-class mIoU results on the Nuscenes test set. Note that our DRINet++ shows result without *Pseudo label*.

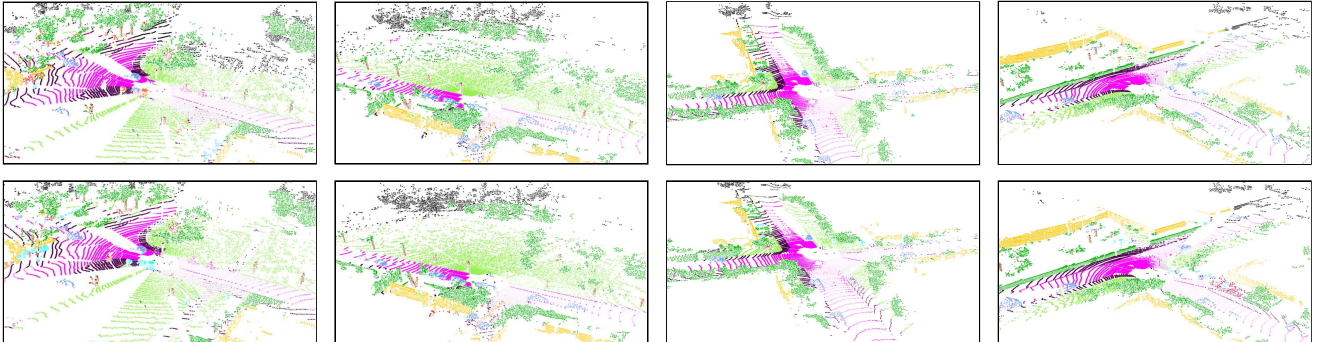


Figure 5. The results on the SemanticKITTI valid set. The top row is the ground truth, and the bottom row is the predictions by DRINet++.

Number of blocks	mIoU (%)	Speed (ms)
1	52.0	26
2	62.3	35
3	68.4	47
4	70.8	59
5	71.2	70

Table 5. Controlled experiments for the number of blocks on the SemanticKITTI validation set.

temporal fusion algorithm, then generate the pointwise output prediction according to Algo. 2. We do not apply any post-processing for refinement. As shown in Tab. 2, our DRINet++ shows a significant improvement compared with previous methods in terms of both metrics. Compared with AF2S3Net [6], which is a voxel-based approach, the proposed method brings a very competitive gain (about 4.4%).

4.3. Results on Nuscenes

To verify the generalization ability of our approach, we also report the results on the test set of the Nuscenes-lidarSeg [3] task. As shown in Tab. 4, our DRINet++ achieves highly competitive results, with 10 out of 16 categories surpassing all other approaches. DRINet++ has a noticeable improvement for classes with small sizes, such as pedestrians and motorcycles. This demonstrates the effectiveness of our sparse geometry feature enhancement, which aims to capture and integrate multi-scale context in-

SFE	SGFE		DSS	Pseudo label	mIoU (%)
	MSP	AMF			
✓					64.5
✓	✓				65.8
✓	✓	✓			67.9
✓	✓	✓	✓		69.4
✓	✓	✓	✓	✓	70.8

Table 6. Ablation study on the SemanticKITTI validation set. MSP refers to Multi-scale Sparse Projection. AMF refers to Attentive Multi-scale Fusion. DSS refers to Deep Sparse Supervision.

formation through hierarchical feature learning and attentive multi-scale fusion.

4.4. Ablation Study

We conduct ablation studies to analyze the effectiveness of each proposed component on the validation set of SemanticKITTI.

Component Study. Our baseline model, shown in Tab. 6, which only uses SFE, has achieved decent performance. This shows that the voxel representation with sparse convolution is highly capable of feature extraction and context information learning in outdoor point cloud semantic segmentation. The MSP layer brings 1.3% improvement with its ability to capture hierarchical geometry information. Furthermore, we apply the AMF to re-distribute the importance of each scale for each channel. This strategy

	VAP	Memory	mIoU (%)
DRINet++	×	2.0 Gb	71.0
	✓	1.4 Gb	70.8
DRINet [56]	×	2.1 Gb	67.3
	✓	1.3 Gb	67.2
SPVCNN [38]	×	2.4 Gb	64.7
	✓	1.9 Gb	64.6

Table 7. Ablation study for the voxel-as-point (VAP) design on the SemanticKITTI validation set.

Method	mIoU(%)
AMF	70.8
Tensor summation	68.8
Tensor concatenation	69.6

Table 8. Ablation study for fusion strategy.

enables the network the focus on the more significant scale and has a performance gain of about 2.1%. Next, adding the deep sparse supervision in the training stage improves the mIoU to 69.4%, an increase of 1.5%. More importantly, this supervision will be disabled when inference, bringing no extra computation cost for deployment. Finally, the data augmentation with pseudo labels shows a promising improvement by leveraging the potential of semi-supervised learning, giving a performance boost of about 1.4%.

Voxel-as-point Analysis. To verify the voxels-as-points (VAP) principle, we compare different models under the VAP and non-VAP settings. As shown in Tab. 7, the VAP design saves about 30% memory usage while only leading to a decrease of about 0.2% mIoU, indicating that the VAP can be a valuable and general principle for the multi-representation framework. By VAP, models can be improved and be lighter without real point representation.

Number of Blocks. We conduct an experiment with various numbers of blocks. As shown in Tab. 5, the mIoU increases from 52.0% to 71.2% when the number of blocks increases to 5 and the runtime nearly doubles. Furthermore, adding one more block when the block number is 4 brings extra 11ms latency and improves mIoU by about 0.4%. Therefore, we choose block number as 4 in our settings.

Scale Feature Fusion Strategy. We analyze the effectiveness of the proposed AMF by comparing it with different fusion strategies. We use tensor concatenation and summation, which are commonly used in feature fusion. For this experiment, we enable all other proposed modules for a fair comparison. As shown in Tab. 8, the AMF layer serves as a better approach for fusing the multi-scale features, which leads to a 2.0% increase compared with the tensor summation. Tab. 10 also shows that other models that utilize multiple representations could benefit from the AMF strategy. Compared with DRINet [56], original SPVCNN [38] does not have hierarchical learning in the

Method	GPU Memory (Mb)	mIoU (%)
Sparse	6	67.9
Dense	552	68.0

Table 9. Ablation study for supervision ways.

Method	Original (%)	DSS (%)	AMF (%)
SPVCNN [38]	64.7	66.1 (+1.4)	66.7 (+2.0)
DRINet [56]	67.3	68.1 (+0.8)	67.9 (+0.6)
Cylinder3D [62]	66.5	67.8 (+1.3)	-

Table 10. Ablation study for DSS on the SemanticKITTI [1] valid set with different models. The statistics are from our reproduction.

pointwise branches, and then its performance will improve when AMF is enabled.

Sparse or Dense Supervision. Deep Sparse supervision is another characteristic of our DRINet++. In this experiment, we compare the sparse and dense supervision in terms of memory cost and performance. We remove the deep auxiliary loss branch for simplicity, with only the main supervision left. The memory consumption for both sparse and dense supervision only includes prediction tensor and label tensor without the consumption used by gradient tensors. As shown in Tab. 9, the memory footprint in sparse supervision only accounts for about one percent of that in dense supervision, and the results are close between the methods. By incorporating sparse supervision, we can use a larger batch size for training, leading to efficient training.

Deep Sparse Supervision. Since our Deep Sparse Supervision is a universal component in the point cloud semantic segmentation task, and we incorporate this strategy with other popular models to verify its effectiveness. As shown in Tab. 10, Deep Sparse Supervision could help the performance of popular models without any extra computation cost for inference.

5. Conclusion

In this paper, we propose DRINet++, an efficient network architecture for point cloud segmentation via the voxel-as-point principle. DRINet++ consists of Sparse Feature Encoder (SFE) and Sparse Geometry Feature Enhancement (SGFE) to fully utilize the sparsity and geometry in a single sparse voxel representation to maintain performance and efficiency. SFE extracts local context information, while SGFE enhances the geometry with multi-scale sparse projection and attentive multi-scale fusion. Moreover, deep sparse supervision is applied to accelerate convergence with a lower memory cost. The experiments on large-scale outdoor datasets show that our approach achieves state-of-the-art performance with impressive runtime efficiency.

References

- [1] Jens Behley, Martin Garbade, Andres Milioto, Jan Quenzel, Sven Behnke, Cyrill Stachniss, and Jurgen Gall. Semantickitti: A dataset for semantic scene understanding of lidar sequences. In *ICCV*, pages 9297–9307, 2019. 2, 5, 8
- [2] Maxim Berman, Amal Rannen Triki, and Matthew B Blaschko. The lovász-softmax loss: A tractable surrogate for the optimization of the intersection-over-union measure in neural networks. In *CVPR*, pages 4413–4421, 2018. 6
- [3] Holger Caesar, Varun Bankiti, Alex H Lang, Sourabh Vora, Venice Erin Liong, Qiang Xu, Anush Krishnan, Yu Pan, Giancarlo Baldan, and Oscar Beijbom. nuscenes: A multimodal dataset for autonomous driving. In *CVPR*, pages 11621–11631, 2020. 2, 5, 7
- [4] Liang-Chieh Chen, George Papandreou, Iasonas Kokkinos, Kevin Murphy, and Alan L Yuille. Deeplab: Semantic image segmentation with deep convolutional nets, atrous convolution, and fully connected crfs. *IEEE transactions on pattern analysis and machine intelligence*, 40(4):834–848, 2017. 3
- [5] Liang-Chieh Chen, George Papandreou, Florian Schroff, and Hartwig Adam. Rethinking atrous convolution for semantic image segmentation. *arXiv preprint arXiv:1706.05587*, 2017. 3
- [6] Ran Cheng, Ryan Razani, Ehsan Taghavi, Enxu Li, and Bingbing Liu. 2-s3net: Attentive feature fusion with adaptive feature selection for sparse semantic segmentation network. In *CVPR*, pages 12547–12556, 2021. 1, 2, 5, 6, 7
- [7] Christopher Choy, JunYoung Gwak, and Silvio Savarese. 4d spatio-temporal convnets: Minkowski convolutional neural networks. In *CVPR*, pages 3075–3084, 2019. 2, 3
- [8] Tiago Cortinhal, George Tzelepis, and Eren Erdal Aksoy. Salsanext: Fast, uncertainty-aware semantic segmentation of lidar point clouds. In *International Symposium on Visual Computing*, pages 207–222. Springer, 2020. 2
- [9] Fabian Duerr, Mario Pfaller, Hendrik Weigel, and Jürgen Beyerer. Lidar-based recurrent 3d semantic segmentation with temporal memory alignment. In *2020 International Conference on 3D Vision (3DV)*, pages 781–790. IEEE, 2020. 6
- [10] Andreas Geiger, Philip Lenz, Christoph Stiller, and Raquel Urtasun. Vision meets robotics: The kitti dataset. *The International Journal of Robotics Research*, 32(11):1231–1237, 2013. 5
- [11] Benjamin Graham, Martin Engelcke, and Laurens Van Der Maaten. 3d semantic segmentation with submanifold sparse convolutional networks. In *CVPR*, 2018. 1, 3, 4
- [12] Meng-Hao Guo, Jun-Xiong Cai, Zheng-Ning Liu, Tai-Jiang Mu, Ralph R Martin, and Shi-Min Hu. Pct: Point cloud transformer. *arXiv preprint arXiv:2012.09688*, 2020. 2
- [13] Kaiming He, Xiangyu Zhang, Shaoqing Ren, and Jian Sun. Deep residual learning for image recognition. In *CVPR*, pages 770–778, 2016. 4
- [14] Jie Hu, Li Shen, and Gang Sun. Squeeze-and-excitation networks. In *CVPR*, pages 7132–7141, 2018. 4
- [15] Qingyong Hu, Bo Yang, Linhai Xie, Stefano Rosa, Yulan Guo, Zhihua Wang, Niki Trigoni, and Andrew Markham. Randla-net: Efficient semantic segmentation of large-scale point clouds. In *CVPR*, pages 11108–11117, 2020. 1, 2, 6
- [16] Diederik P Kingma and Jimmy Ba. Adam: A method for stochastic optimization. *arXiv preprint arXiv:1412.6980*, 2014. 6
- [17] Sudhakar Kumawat and Shanmuganathan Raman. Lp-3dcnn: Unveiling local phase in 3d convolutional neural networks. In *CVPR*, pages 4903–4912, 2019. 2
- [18] Truc Le and Ye Duan. Pointgrid: A deep network for 3d shape understanding. In *CVPR*, pages 9204–9214, 2018. 2
- [19] Dong-Hyun Lee et al. Pseudo-label: The simple and efficient semi-supervised learning method for deep neural networks. In *Workshop on challenges in representation learning, ICML*, volume 3, page 896, 2013. 6
- [20] Xiang Li, Wenhai Wang, Xiaolin Hu, and Jian Yang. Selective kernel networks. In *CVPR*, pages 510–519, 2019. 4, 5
- [21] Yangyan Li, Rui Bu, Mingchao Sun, Wei Wu, Xinhan Di, and Baoquan Chen. Pointcnn: Convolution on x-transformed points. *Advances in neural information processing systems*, 31:820–830, 2018. 2
- [22] Ze Liu, Han Hu, Yue Cao, Zheng Zhang, and Xin Tong. A closer look at local aggregation operators in point cloud analysis. In *ECCV*, pages 326–342. Springer, 2020. 2
- [23] Zhijian Liu, Haotian Tang, Yujun Lin, and Song Han. Point-voxel cnn for efficient 3d deep learning. In *Advances in Neural Information Processing Systems*, pages 965–975, 2019. 1, 2, 3, 4
- [24] Jonathan Long, Evan Shelhamer, and Trevor Darrell. Fully convolutional networks for semantic segmentation. In *CVPR*, pages 3431–3440, 2015. 3, 5
- [25] Antonio Loquercio, Alexey Dosovitskiy, and Davide Scaramuzza. Learning depth with very sparse supervision. *IEEE Robotics and Automation Letters*, 5(4):5542–5549, 2020. 5
- [26] Andrew L Maas, Awni Y Hannun, Andrew Y Ng, et al. Rectifier nonlinearities improve neural network acoustic models. In *Proc. icml*, volume 30, page 3. Citeseer, 2013. 4
- [27] Daniel Maturana and Sebastian Scherer. Voxnet: A 3d convolutional neural network for real-time object recognition. In *IROS*, pages 922–928. IEEE, 2015. 2
- [28] Andres Milioto, Ignacio Vizzo, Jens Behley, and Cyrill Stachniss. Rangenet++: Fast and accurate lidar semantic segmentation. In *IROS*, pages 4213–4220. IEEE, 2019. 3
- [29] Andres Milioto, Ignacio Vizzo, Jens Behley, and Cyrill Stachniss. Rangenet++: Fast and accurate lidar semantic segmentation. In *IROS*, pages 4213–4220. IEEE, 2019. 6
- [30] Quang-Hieu Pham, Thanh Nguyen, Binh-Son Hua, Gemma Roig, and Sai-Kit Yeung. Jsis3d: Joint semantic-instance segmentation of 3d point clouds with multi-task pointwise networks and multi-value conditional random fields. In *CVPR*, pages 8827–8836, 2019. 2
- [31] Charles R Qi, Hao Su, Kaichun Mo, and Leonidas J Guibas. Pointnet: Deep learning on point sets for 3d classification and segmentation. In *CVPR*, pages 652–660, 2017. 1, 2, 6
- [32] Charles Ruizhongtai Qi, Li Yi, Hao Su, and Leonidas J Guibas. PointNet++: Deep Hierarchical Feature Learning

- on Point Sets in a Metric Space. In *Advances in Neural Information Processing Systems 30*, volume 30, pages 5099–5108. Curran Associates, Inc., 2017. [1](#), [2](#), [4](#), [6](#)
- [33] Xiaojuan Qi, Renjie Liao, Jiaya Jia, Sanja Fidler, and Raquel Urtasun. 3d graph neural networks for rgb-d semantic segmentation. In *ICCV*, pages 5199–5208, 2017. [2](#)
- [34] Olaf Ronneberger, Philipp Fischer, and Thomas Brox. U-net: Convolutional networks for biomedical image segmentation. In *International Conference on Medical image computing and computer-assisted intervention*, pages 234–241. Springer, 2015. [3](#)
- [35] Radu Alexandru Rosu, Peer Schütt, Jan Quenzel, and Sven Behnke. Latticenet: Fast point cloud segmentation using permutohedral lattices. *arXiv preprint arXiv:1912.05905*, 2019. [6](#)
- [36] Hang Su, Subhransu Maji, Evangelos Kalogerakis, and Erik Learned-Miller. Multi-view convolutional neural networks for 3d shape recognition. In *ICCV*, pages 945–953, 2015. [2](#)
- [37] Ke Sun, Bin Xiao, Dong Liu, and Jingdong Wang. Deep high-resolution representation learning for human pose estimation. In *CVPR*, pages 5693–5703, 2019. [3](#)
- [38] Haotian Tang, Zhijian Liu, Shengyu Zhao, Yujun Lin, Ji Lin, Hanrui Wang, and Song Han. Searching efficient 3d architectures with sparse point-voxel convolution. In *ECCV*, pages 685–702. Springer, 2020. [1](#), [2](#), [3](#), [4](#), [6](#), [7](#), [8](#)
- [39] Maxim Tatarchenko, Jaesik Park, Vladlen Koltun, and Qian-Yi Zhou. Tangent convolutions for dense prediction in 3d. In *CVPR*, pages 3887–3896, 2018. [6](#)
- [40] Gusi Te, Wei Hu, Amin Zheng, and Zongming Guo. Rgcnn: Regularized graph cnn for point cloud segmentation. In *Proceedings of the 26th ACM international conference on Multimedia*, pages 746–754, 2018. [2](#)
- [41] Hugues Thomas, Charles R Qi, Jean-Emmanuel Deschaud, Beatriz Marcotegui, François Goulette, and Leonidas J Guibas. Kpconv: Flexible and deformable convolution for point clouds. In *ICCV*, pages 6411–6420, 2019. [2](#), [4](#), [6](#)
- [42] Ozan Unal, Luc Van Gool, and Dengxin Dai. Improving point cloud semantic segmentation by learning 3d object detection. In *WACV*, pages 2950–2959, 2021. [3](#), [6](#)
- [43] Chu Wang, Babak Samari, and Kaleem Siddiqi. Local spectral graph convolution for point set feature learning. In *ECCV*, pages 52–66, 2018. [2](#)
- [44] Lei Wang, Yuchun Huang, Yaolin Hou, Shenman Zhang, and Jie Shan. Graph attention convolution for point cloud semantic segmentation. In *CVPR*, pages 10296–10305, 2019. [2](#)
- [45] Yue Wang, Yongbin Sun, Ziwei Liu, Sanjay E Sarma, Michael M Bronstein, and Justin M Solomon. Dynamic graph cnn for learning on point clouds. *Acm Transactions On Graphics (tog)*, 38(5):1–12, 2019. [2](#)
- [46] Bichen Wu, Alvin Wan, Xiangyu Yue, and Kurt Keutzer. SqueezeSeg: Convolutional neural nets with recurrent crf for real-time road-object segmentation from 3d lidar point cloud. In *ICRA*, pages 1887–1893. IEEE, 2018. [2](#)
- [47] Wenxuan Wu, Zhongang Qi, and Li Fuxin. Pointconv: Deep convolutional networks on 3d point clouds. In *CVPR*, pages 9621–9630, 2019. [2](#)
- [48] Chenfeng Xu, Bichen Wu, Zining Wang, Wei Zhan, Peter Vajda, Kurt Keutzer, and Masayoshi Tomizuka. SqueezeSegv3: Spatially-adaptive convolution for efficient point-cloud segmentation. In *ECCV*, pages 1–19. Springer, 2020. [2](#), [6](#)
- [49] Jianyun Xu, Ruixiang Zhang, Jian Dou, Yushi Zhu, Jie Sun, and Shiliang Pu. Rpvnet: A deep and efficient range-point-voxel fusion network for lidar point cloud segmentation. *arXiv preprint arXiv:2103.12978*, 2021. [1](#), [3](#), [6](#)
- [50] Qiangeng Xu, Xudong Sun, Cho-Ying Wu, Panqu Wang, and Ulrich Neumann. Grid-gcn for fast and scalable point cloud learning. In *CVPR*, pages 5661–5670, 2020. [2](#)
- [51] Xu Yan, Jiantao Gao, Jie Li, Ruimao Zhang, Zhen Li, Rui Huang, and Shuguang Cui. Sparse single sweep lidar point cloud segmentation via learning contextual shape priors from scene completion. *arXiv preprint arXiv:2012.03762*, 2020. [2](#), [6](#)
- [52] Yan Yan, Yuxing Mao, and Bo Li. Second: Sparsely embedded convolutional detection. *Sensors*, 18(10):3337, 2018. [1](#), [3](#), [4](#)
- [53] Maoke Yang, Kun Yu, Chi Zhang, Zhiwei Li, and Kuiyuan Yang. Denseaspp for semantic segmentation in street scenes. In *CVPR*, pages 3684–3692, 2018. [3](#)
- [54] Maosheng Ye, Tongyi Cao, and Qifeng Chen. Tpcn: Temporal point cloud networks for motion forecasting. In *Proceedings of the IEEE/CVF Conference on Computer Vision and Pattern Recognition*, pages 11318–11327, 2021. [1](#)
- [55] Maosheng Ye, Shuangjie Xu, and Tongyi Cao. Hynet: Hybrid voxel network for lidar based 3d object detection. In *CVPR*, pages 1631–1640, 2020. [3](#)
- [56] Maosheng Ye, Shuangjie Xu, Tongyi Cao, and Qifeng Chen. Drinet: A dual-representation iterative learning network for point cloud segmentation. In *ICCV*, 2021. [1](#), [2](#), [3](#), [4](#), [6](#), [8](#)
- [57] Kuangen Zhang, Ming Hao, Jing Wang, Clarence W de Silva, and Chenglong Fu. Linked dynamic graph cnn: Learning on point cloud via linking hierarchical features. *arXiv preprint arXiv:1904.10014*, 2019. [2](#)
- [58] Yingxue Zhang and Michael Rabbat. A graph-cnn for 3d point cloud classification. In *2018 IEEE International Conference on Acoustics, Speech and Signal Processing (ICASSP)*, pages 6279–6283. IEEE, 2018. [2](#)
- [59] Yang Zhang, Zixiang Zhou, Philip David, Xiangyu Yue, Zerong Xi, Boqing Gong, and Hassan Foroosh. Polarnet: An improved grid representation for online lidar point clouds semantic segmentation. In *CVPR*, pages 9601–9610, 2020. [2](#), [3](#), [5](#), [6](#), [7](#)
- [60] Hengshuang Zhao, Li Jiang, Jiaya Jia, Philip Torr, and Vladlen Koltun. Point transformer. *arXiv preprint arXiv:2012.09164*, 2020. [2](#)
- [61] Hengshuang Zhao, Jianping Shi, Xiaojuan Qi, Xiaogang Wang, and Jiaya Jia. Pyramid scene parsing network. In *CVPR*, pages 2881–2890, 2017. [3](#), [4](#)
- [62] Xinge Zhu, Hui Zhou, Tai Wang, Fangzhou Hong, Yuexin Ma, Wei Li, Hongsheng Li, and Dahua Lin. Cylindrical and asymmetrical 3d convolution networks for lidar segmentation. In *CVPR*, pages 9939–9948, 2021. [1](#), [2](#), [3](#), [5](#), [6](#), [7](#), [8](#)